RSC Advances

ROYAL SOCIETY OF CHEMISTRY

www.rsc.org/advances

Graphical abstract for the paper

Non-aqueous preparation of $LaPO_4$ nanoparticles and their application for ethanol dehydration.

By P. Afanasiev.

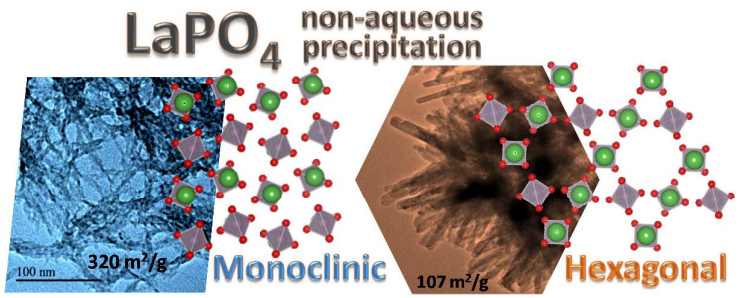

Synopsis sentences:

Control of phase polymorph and morphology of $LaPO_4$ has been achieved in room temperature non-aqueous precipitations by changing the nature of solvent. Hexagonal variety of $LaPO_4$ shows high performance in ethanol dehydration.

Non-aqueous preparation of $LaPO_4$ nanoparticles and their application for ethanol dehydration.

Pavel Afanasiev[a]

Abstract.

Nanodispersed single phase monoclinic and hexagonal $LaPO_4$ materials have been prepared in polar non-aqueous solvents at room temperature, by means of precursor salts metathesis. The morphology and phase composition strongly depend on the nature of non-aqueous solvent. Reaction in propylene carbonate produced hexagonal $LaPO_4$ nanorods; formamide gave monolith gel of monoclinic phase, whereas reaction in ethylene glycol led to formation of stable colloidal suspension of M-$LaPO_4$. Outstandingly high specific surface areas of materials allow their use as soft acidic catalytic materials for highly selective dehydration of ethanol. Comparison of catalytic properties reveals the importance of phase polymorph, hexagonal $LaPO_4$ demonstrating better catalytic performance than monoclinic phase.

Introduction

Lanthanum phosphate is an important material in science and technology. As a material for optics, lanthanum phosphate is an attractive host for phosphors doped with rare earth ions such as Ce, Tb and Eu.[1,2,3]. Monoclinic $LaPO_4$ (monazite) has advantageous properties for ceramics applications.[4,5,6] Doped $LaPO_4$ is an efficient ionic conductor.[7,8,9] Low solubility and refractory properties of monazite allow considering it as a host for radioactive wastes storage.[10] During the last years $LaPO_4$ was widely studied as a catalyst. Thus, we reported that $LaPO_4$ prepared topotactically from LaOCl is a soft acidic catalyst, highly selective to dehydration of isopropanol.[11] Advantage of moderate acidity provided by $LaPO_4$ was evidenced for oxidative dehydrogenation of butane[12] and formation of acetal.[13] Hexagonal

$LaPO_4$ nanorods synthesized by hydrothermal method were applied as a novel catalyst for photocatalytic reduction of CO_2 with H_2O under mild conditions.[14] Recently the properties of different $LaPO_4$ preparations were studied in the dehydration of ethanol and butanol and high selectivity to olefins formation was achieved.[15]

Due to its importance for the materials chemistry, a great body of work has been published on the preparation of $LaPO_4$ with controlled properties. Hydrothermal,[16] mechanochemical,[17] solvothermal,[18] polyol[19] and many other methods were applied. Solution routes using precipitation from lanthanum nitrate and orthophosphoric acid yield hexagonal $LaPO_4$ (rhabdophane) that typically exhibits needle-like particle morphology and contains excess phosphorus.[20] Solution preparation of monoclinic $LaPO_4$ (monazite) is more challenging. Solvothermal method applying tris(ethylhexyl) phosphate allowed preparation of 5 nm size monazite.[21] Alternatively, pure monazite phase could be prepared by direct water-free precipitation from phosphoric acid and lanthanum chloride.[22]

Here we report on the non-aqueous preparation of $LaPO_4$ nanoparticles with the possibility of phase and morphology control by varying a non-aqueous solvent. Catalytic properties of as obtained $LaPO_4$ materials are compared in the ethanol dehydration.

2. Experimental

2.1. Materials preparation

High purity grade diammonium hydrophosphate and hexahydrated lanthanum chloride from Aldrich were applied as precursors in all syntheses. All solvents were high purity grade purchased from Aldrich. An equimolar mixture containing 0.025 mol of each salt was loaded in a flask and then 25 ml of a non-aqueous solvent was added. Then the mixture was kept under 300 min^{-1} stirring for 8 hours at its own pH. The obtained solids were separated, twice

washed with the reaction solvent, ethanol, and acetone and then dried at room temperature. Such complex washing procedure was applied to remove inorganic products of metathesis and eventual impurities of non-reacted precursors, avoiding any possible modification of morphology by water. Stable colloidal suspension formed in ethylene glycol was flocculated by acetone. Monolith gel formed in the formamide solution was cut into pieced and soaked many times with ethanol, then acetone, and finally hexane. Hexane was evaporated under ambient conditions. The samples prepared in propylene carbonate (PRC), ethylene glycol (EG) and formamide (FA) are designated respectively $LaPO_4$-PRC, $LaPO_4$-EG and $LaPO_4$-FA.

2.2. Characterizations

X-ray diffraction (XRD) patterns were obtained on a Bruker diffractometer with Ni-filtered Cu Kα radiation, in the range of 2θ between 3° and 80°. Crystalline phases were identified by comparison with standard ICDD files. Particle size was calculated using the Scherrer formula. The morphology and composition were examined by transmission electron microscopy (TEM), high-resolution transmission electron microscopy (HRTEM) energy dispersive spectroscopy (EDS) and selected area electron diffraction (SAED) on a JEOL 2010 microscope with an accelerating voltage of 200 kV. For TEM analysis, the nanoparticles were dispersed in ethanol by ultrasound. Then, a drop of suspension was transferred to a holey carbon film supported on a copper grid and evaporated naturally.

Surface areas and pore radii distributions were measured by low temperature (-196 °C) nitrogen adsorption and calculated using BET equation for specific surface area, BJH for mesopores and Horvath-Kawazoe equation for micropores distribution. Pore size disctributions were calculated from desorption branch of isotherms. For microporosity measurements, small variable pressure step of nitrogen pressure was applied to have 25 points

in the range of P/P0 from 10^{-6} to 0.1. Prior to measurements the samples were outgased for 4 h at 400°C under secondary vacuum about 0.01 Pa.

The distribution of Brønsted acid sites was investigated by temperature-programmed desorption (TPD) measurements of NH_3. To carry out the TPD, a $LaPO_4$ sample (about 0.1 g) was placed in a quartz reactor, preheated in Ar flow at 100°C and saturated with a flow of ammoniac (50 $mL.min^{-1}$). Then physisorbed ammoniac was flushed away at 100°C with argon flow and the sample was kept in Ar while being cooled to room temperature, for 30 min. Then the TPD profile was detected by heating of reactor form RT to 600 °C at 10 $°min^{-1}$ rate. The amount of NH_3 was monitored with a Thermo Prolab mass-spectrometer at m/z 17, 16 and 15. These multiple m/z signals were followed to unravel the signal of NH_3 from that of water, always present as a strong background.

2.3. Catalytic tests.

Ethanol conversion was studied at atmospheric pressure between 290 and 360 °C in a fixed-bed down-flow reactor. Weighted amount of $LaPO_4$ catalyst (100±2 mg) was packed into a glass microreactor and the alcohol vapor was introduced using high purity nitrogen carrier gas flow (50 $mL.min^{-1}$), flowing through an evaporator–saturator system placed in a cryostat at 0 °C. All tests have been done at W/F 44±1 $g_{cata}.h.mol^{-1}$. The reaction products were analyzed online by gas chromatography using a HP 5890 device and Agilent ChemStation software. Ethanol and diethyl ether were the principal reaction products, with carbon balance better than 98%. The catalytic properties of lanthanum phosphates have been compared to an Al_2O_3 industrial reference, as reported in the previous work [15].

3. Results and discussion

3.1. Behavior of the reaction mixtures.

Reaction mixtures behaved differently as a function of non-aqueous solvent applied for synthesis. The values of measured pH were near 6.1 for EG and 6.5 for FA, whereas for aprotic PRC pH value cannot be reliably determined. Acidic solvilysis of $LaCl_3$ (aqueous pH 4.7) and of $(NH_4)_2HPO_4$ (aqueous pH 8.1) occur in the protic solvents and compensate each other, leading to nearly neutral pH. In propylene carbonate (PRC) slow dissolution of precursor's crystals occurred with simultaneous buildup of milky opacity. After several hours of stirring a white suspension was formed, which rapidly decanted when stirring was stopped. In ethylene glycol (EG) complete dissolution of both precursors was observed. Opalescence appeared increased progressively after approximately one hour of stirring and. After 8 h there was no evolution of the reaction mixture: a colloidal suspension was formed, stable for indefinite time. Blending in formamide (FA) resulted in complete dissolution of both precursors followed by simultaneous increase of viscosity of the reaction mixture, seen as progressive slowing down of the stirrer rotation. After several hours the stirring spontaneously stopped because monolith transparent (but slightly opaque) gel was formed.

Under the same conditions of blending, the reaction using water as a solvent was immediate, with instant formation of white precipitate. Therefore non-aqueous solvents provide much slower nucleation kinetics (and probably better possibilities of control).

3.2 Morphology and phase composition of the solids.

Powder XRD study showed that all three solids are single-phase and contain monoclinic $LaPO_4$ monazite phase for $LaPO_4$-EG and $LaPO_4$-FA or hexagonal rhabdophane for $LaPO_4$-PRC (Fig. 1). Therefore in all solvents the same precipitation reaction occurred, according to eq. 1

$$(NH_4)_2HPO_4 + LaCl_3 \rightarrow LaPO_4 + 2NH_4Cl + HCl \quad (1)$$

As follows from the equation (1), acidity should rise during the precipitation. However, lanthanum phosphate is insoluble in diluted acids.

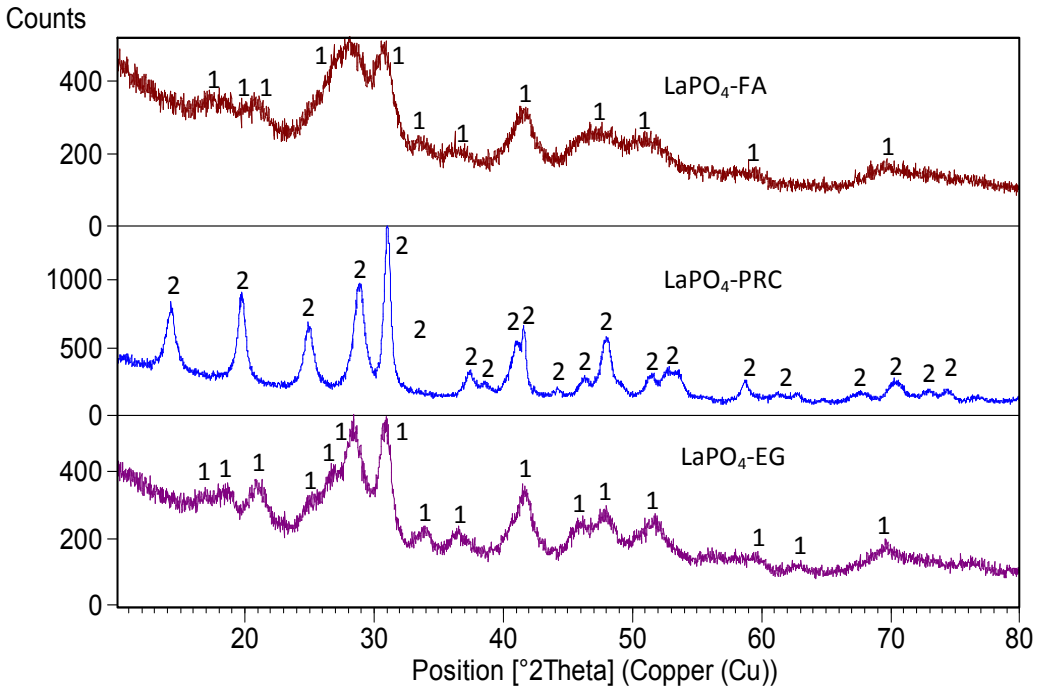

Fig. 1 XRD patterns of $LaPO_4$ prepared in FA, PRC and EG. For LaPO4-FA and $LaPO_4$- EG all peaks correspond to M-$LaPO_4$ (label 1; JCPDS 00-012-0283); for $LaPO_4$-PRC all lines are identified as rhabdophane (label 2; JCPDS 01-075-1881).

Very broad XRD lines and the absence of standalone single-reflection lines make difficult determination of particle size from the XRD patters of monazite samples. Particle size derived from Scherrer for $LaPO_4$–PRC was 8±1 nm for (200) line and 18±1 nm for (102) line, indicating acicular shape of particles.

Transmission electron microscopy shows strong difference of morphology between the $LaPO_4$ samples prepared in different solvents. $LaPO_4$-FA has aerogel-like morphology i.e. loose

porous structure formed by fiber-like agglomerates of $LaPO_4$ particles. Note that formamide and N-methylformamde are prone to formation of gels as observed earlier for sulfides.[23]

The solid prepared in EG consists of agglomerated small aspect ratio particles. PRC preparation represents relatively dense urchin-like agglomerates of $LaPO_4$ rods. Aqueous preparation has shapeless particles intermingled with some rhabdophane nanorods (Fig. 2).

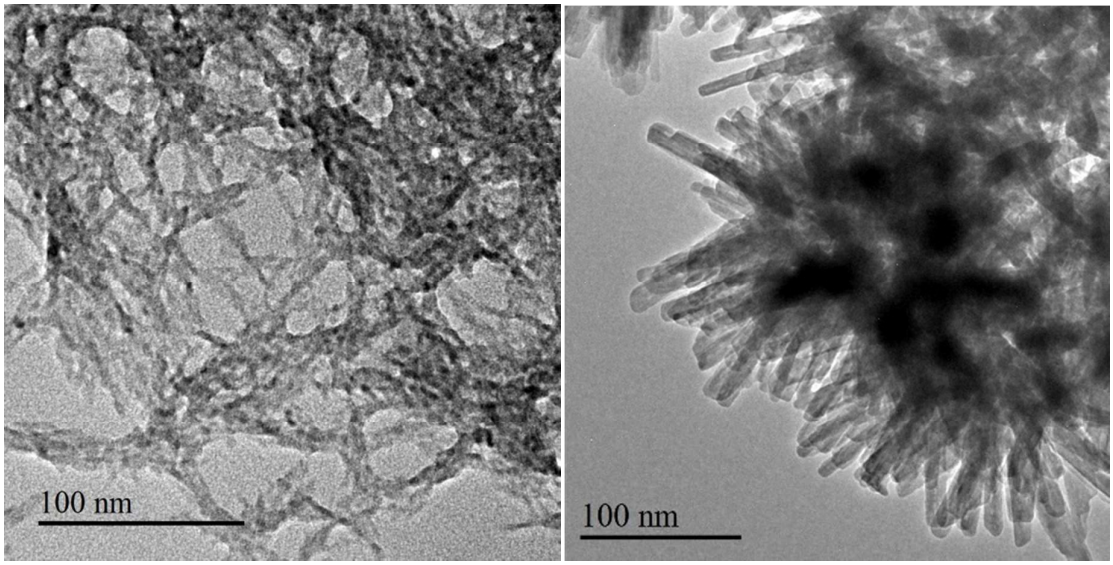

(a) $LaPO_4$-FA (b) $LaPO_4$-PRC

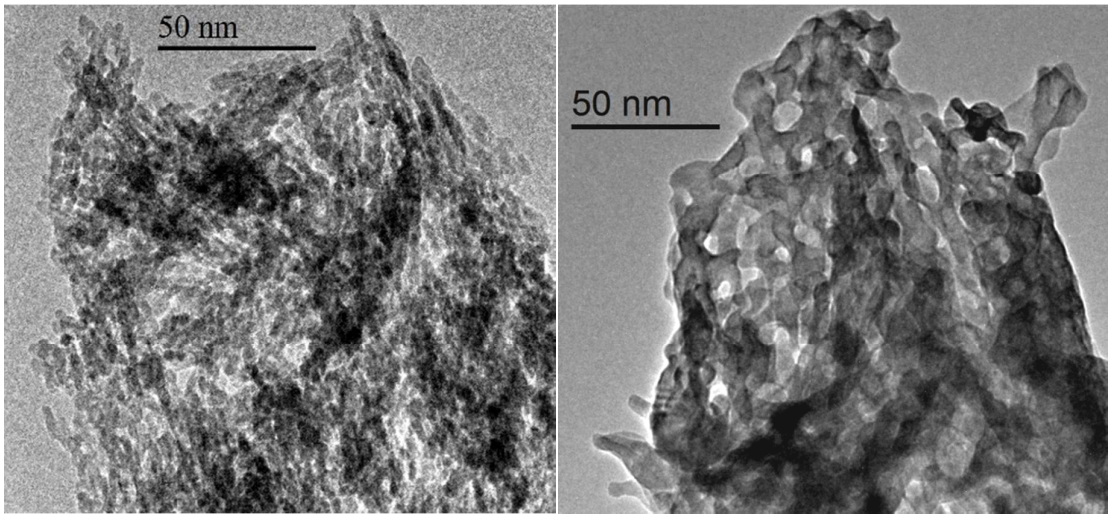

(c) $LaPO_4$-EG (d) $LaPO_4$-H_2O

Fig. 2. TEM images of $LaPO_4$ prepared in non-aqueous solvents and in water.

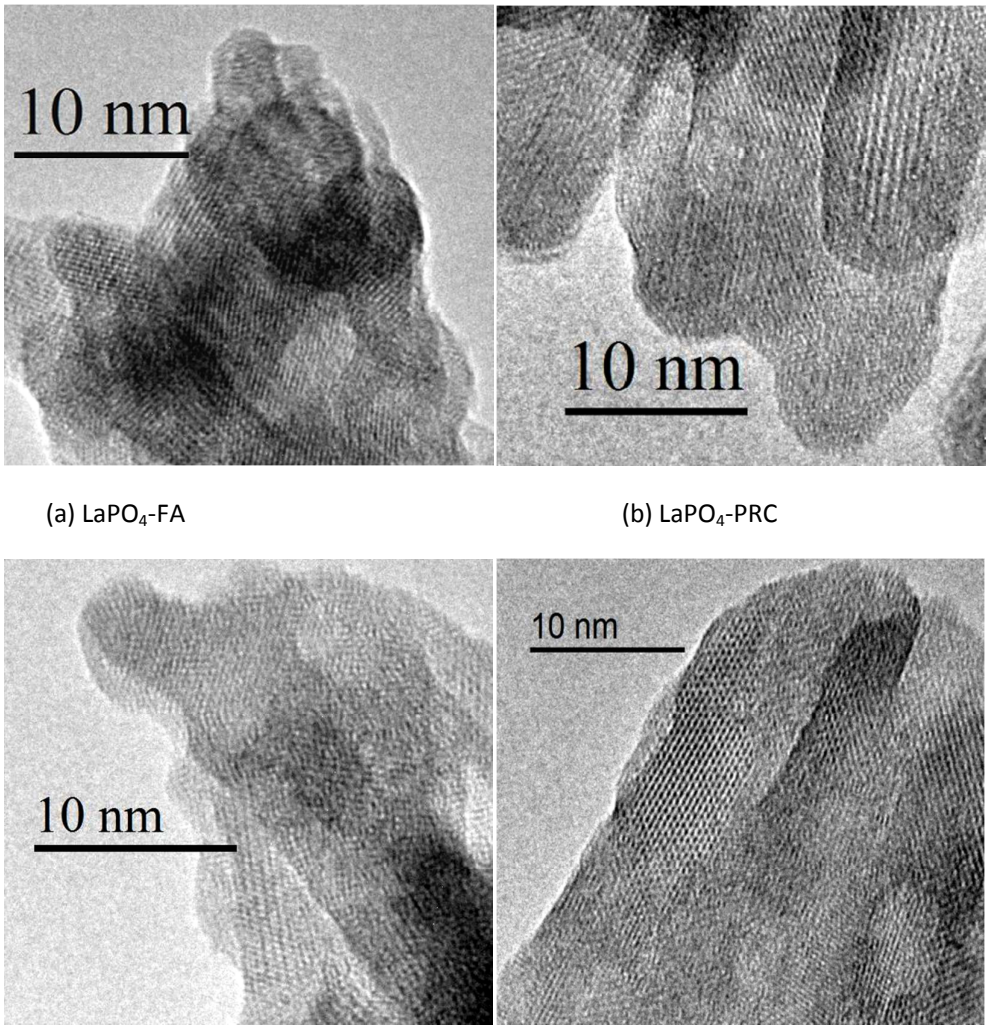

(a) $LaPO_4$-FA (b) $LaPO_4$-PRC

(b) $LaPO_4$-EG (d) $LaPO_4$-H_2O

Fig. 3 HREM images of the $LaPO_4$ solids.

HRTEM (Fig. 3) reveals orientation of rhabdophane nanorods along [001] axis (i.e. perpendicularly to the (001) plane, containing "zeolitic" channels), usual for this type of materials (Fig. 3b). Monazite particles in $LaPO_4$-FA are nearly isotropic (Fig. 3a), whereas $LaPO_4$-EG has acicular primary particles (Fig. 3c). All non-aqueous samples are fully crystalline, no amorphous matter (unseen by XRD) could be observed by TEM. EDS analysis shows La:P ratio close to 1 in all non-aqueous samples. Indeed, the La:P ratio in the reaction

mixtures was strictly equimolar and the yields were quantitative. Therefore the La:P ratio of 1 is preserved in non-aqueous preparations. In contrast to non-aqueous samples, aqueous preparation $LaPO_4$-H_2O showed and overall La/P ratio of 1.2. That probably occurs dure to more advanced hydrolysis of La(III) ions in water, leading to partial precipitation of amorphous hydroxophosphate as minor impurity. Residual chloride from the $LaCl_3$ precursor was below 0.1% for $LaPO_4$-PRC and 0.2% for $LaPO_4$-FA and $LaPO_4$-EG.

The differences in the precipitates morphology correlate with the properties of the liquids. Less interacting aprotic PRC produced larger and easily separable particles. Strongly solvating protic EG and FA produced fine dispersions in which strong interaction with the solvent persisted in the final reaction products, in the form of the stable colloid or of the transparent gel. In a similar way polymorph-directing influence of the solvent nature might be explained. Supposedly, relatively weakly interacting aprotic PRC is unable to expulse water (initially present in the hydrated precursor) from the coordination sphere of La(III) ions. By contrast, strongly interacting and forming hydrogen bonds FA and EG totally replace water in the dissolved La species and then produce anhydrous polymorph. Indeed, water-free precipitation is necessary to produce monazite, as pointed in ref. [22]. The problem certainly merits further study. However, physical events relevant to nucleation as ion association and formation of solvates should be considered in their relative dynamics, which is a challenge. Ion pairing La(III) vs. solvation in aqueous solutions was recently studied by THz spectroscopy.[24] Nucleation of different polymorphs vs. the solvent nature might also be addressed by molecular dynamics, though this is a hard problem, both conceptually and computationally.

The materials as prepared show the highest specific surface area ever reported for $LaPO_4$ materials, namely 320±10 m^2/g for $LaPO_4$-FA and 225±8 m^2/g for $LaPO_4$-EG. Specific

surface area of $LaPO_4$ – PRC was 107±5 m^2/g, which is high, but lies in the usual range of the specific surface values obtained for this phase in aqueous medium [15]. Aqueous sample $LaPO_4$-H_2O has lower specific surface area of 46±5 m^2/g in agreement with its larger primary particles and their strong agglomeration, as seen by TEM.Commercial $LaPO_4$ purchased from Aldrich and Alfa Aesar had specific surface area of 51 m^2/g and 38 m^2/g, respectively.

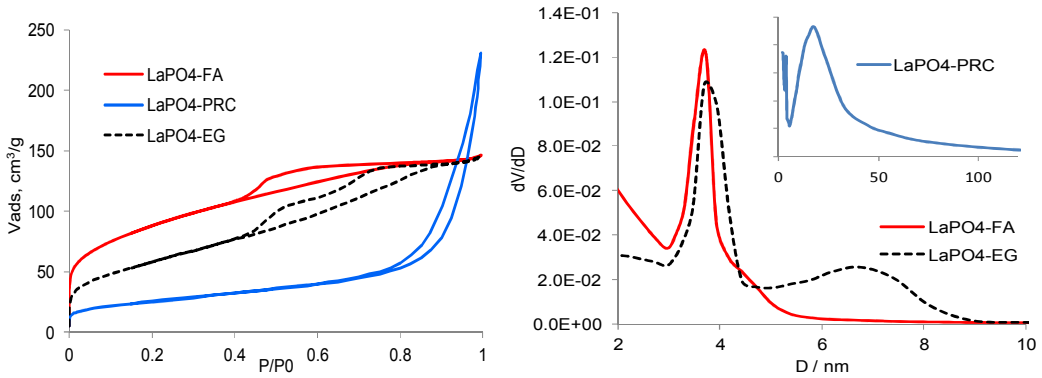

(a) (b)

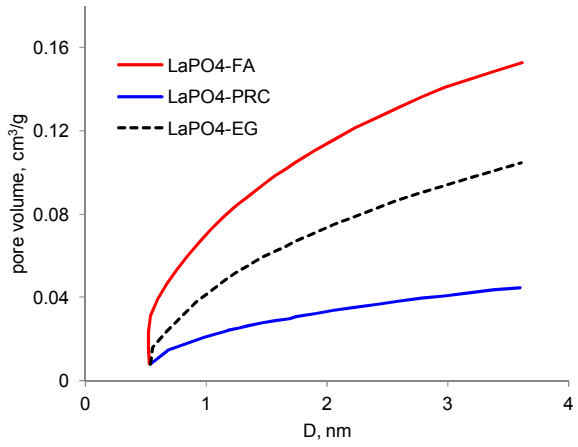

(c)

Fig. 4. Nitrogen adsorption-desorption isotherms (a) and BJH pore volume distributions (b) and Horvath-Kawazoe cumulative pore volume (c) for the $LaPO_4$ solids.

Monazite nanodispersions $LaPO_4$-FA and $LaPO_4$-EG show IV type isotherms with H2 type hysteresis. Rhabdophane $LaPO_4$-PRC has type III isotherm with H3 hysteresis loop,

suggesting weaker interaction of adsorbate with the solid and the presence of large mesopores. Pore volume distribution analysis had shown that $LaPO_4$-PRC is essentially mesoporous with the total pore volume of 0.35 cm^3/g (BJH mean pore diameter 15.5 nm) and micropore volume of only 0.004 cm^3/g.

According to TEM study, $LaPO_4$-EG is strongly agglomerated and by this reason it has the lowest pore volume of total 0.22 cm^3/g (BJH desorption average pore diameter 4.1867 nm) of which micropores represent 0.10 cm^3/g.

$LaPO_4$-FA derived from monolith gel demonstrated the lowest apparent density of powder and showed open framework structure in TEM. However its total BJH pore volume appeared surprisingly low, of only 0.24 cm^3/g (BJH pore size of 3.0 nm), including 0.16 cm^3/g of micropores. It seems that the wide openings seen in $LaPO_4$-FA by TEM are not detected as pores by nitrogen adsorption, because of their loose consistence, unable to form a meniscus.

The lower closure point of hysteresis in $LaPO_4$-FA and $LaPO_4$-EG in Fig. 4b is determined by the tensile strength of the capillary condensed N_2 in small mesopores, where exists a mechanical stability limit, below which a liquid meniscus is unstable and spontaneous N_2 evaporation occurs. This leads to an artificial step in the desorption isotherm, generating a pore size distribution artifact near 4 nm. More appropriate Horwath-Kawazoe treatment of low-pressure parts of isotherms ($P/P0 < 0.3$) shows that micropore volume changes in the order $LaPO_4$-FA > $LaPO_4$-EG > $LaPO_4$-PRC (Fig. 4c).

In summary, non-aqueous metathesis yields $LaPO_4$ materials with small particles size and high specific surface areas. Though not uniform-size, the materials prepared by non-aqueous metathesis usually have narrow and sharply peaked particle size distributions. Meanwhile, reaction conditions control in our syntheses is minimal. In contrast to nonaqueous preparations, blending of the same precursors in water leads to larger primary particles

forming tight micron-size agglomerates. The explanation of advantages of non-aqueous metathesis (not limited to $LaPO_4$ materials) will be discussed in detail elsewhere. Here we only note that the key point is slow nucleation in these polar solvents. Due to strong ion pairing in the non-aqueous liquids, the major part of the precursor species is bound within ionic associates and their release becomes a limiting step, making the nucleation orders of magnitude slower, as compared with water. Under such conditions, small and narrow size distributed particles tend to be formed.

3.3. Catalytic activity in the ethanol dehydration.

The dehydration of ethanol attracted significant attention to produce ethylene and diethyl ether from non-petroleum renewable feedstock including bioethanol.[25] Dehydration can proceed leading to ethylene (eq. 2), diethyl ether (eq. 3) or to give secondary products with higher numbers of carbon. The most valuable product is ethylene as it represents a widely applied source for versatile petrochemicals.

$$C_2H_5OH \rightarrow C_2H_4+H_2O \quad (2)$$

$$2C_2H_5OH \rightarrow (C_2H_5)O +H_2O \quad (3)$$

Ethanol dehydration was studied on zeolite catalysts including HZSM-5 [26] and SAPO.[27] Zeolithes allow the reaction to occur near 300 °C with high conversion and high selectivity. However strong and non-uniform acid sites lead to undesirable by-products and significant coking. To remediate this drawback HZSM-5 was modified by phosphorous[28] or by rare earths.[29] Aluminas have also been used for dehydration of ethanol.[30,31] Currently this reaction attracts renewed interest in view of converting to ethylene bioethanol produced by fermentation. Actively developed complementary approach considers membrane-assisted processes, when a catalyst is embedded into a semi-transparent membrane.[32,33]

In the recent paper [15] several hexagonal $LaPO_4$ solids have been compared, differing by synthesis method and La/P ratio. It was supposed that the activity and stability are defined by the La/P ratio in the solids as well as the degree of dispersion of subsurface extraneous phosphoric species. Here we compare three catalysts differing by morphology and phase polymorph.

Hexagonal $LaPO_4$ contains variable amounts of water in the "zeolitic" channels parallel to [001] axis of the structure, whereas monazite structure is more compact and cannot adopt water molecules.[34] Rhabdophane can be irreversibly transformed to monazite by dehydration at elevated temperature above 600 °C.[35,36] In order to unravel the influence of morphology from that of the nature of polymorph, we obtained monazite nanorods by heating the $LaPO_4$-PRC solid in air flow at 700 °C for 4h. TEM and texture study (not shown) evidenced that the nanorods fully retained their morphology after calcination, whereas specific surface area decreased slightly, from 107 to 99 m^2/g. Observed low sintering agrees with well-known refractory properties of $LaPO_4$.

The catalytic properties of three monazite solids, one rhabdophane catalyst and alumina reference are presented in Fig. 5. Rhabdophane $LaPO_4$-PRC showed the best activity and selectivity. Ultra-selectivity to ethylene (important for this process) was observed for $LaPO_4$-PRC. At the 99% conversion, the selectivity of $LaPO_4$-PRC was better than 99.6%. Other solids showed lower performance. These figures compare to the most active rhabdophane samples prepared in aqueous medium (though using not just simple metathesis, but elaborated special techniques).[15] Despite its triply higher specific surface area, $LaPO_4$-FA demonstrated lower catalytic activity than $LaPO_4$-PRC, being at the same level as commercial alumina reference, whereas the $LaPO_4$-EG catalyst was an outsider. After transformation to monazite by thermal treatment, $LaPO_4$-PRC solid had lost its advantageous catalytic performance and

thermally treated solid $LaPO_4$-PRC-700° become similar to $LaPO_4$-EG by its catalytic properties. Therefore, phase polymorph plays more important role for good activity and high selectivity to ethylene, than the specific surface area of the $LaPO_4$ materials. Low surface area rhabrophane $LaPO_4$-H_2O and commercial monazite from Aldrich demonstrated poor catalytic performance (not shown).

The thermal stability of the hydrate water in the channels of $LaPO_4$ rhabdophane is important for its good proton conductivity.[9] Though ionic conduction and catalytic turnover are different phenomena, they are both dynamic processes and are sometimes well correlated, as e.g. for some types of oxidation catalysis.[37] It can be supposed that the ability of hexagonal $LaPO_4$ to accommodate water might be useful for elimination of water molecules produced in the reaction via the "zeolithic" tunnels of rhabdophane and therefore to be beneficial for the catalytic performance. To verify this hypothesis, precise models of catalytic site should be built and checked.

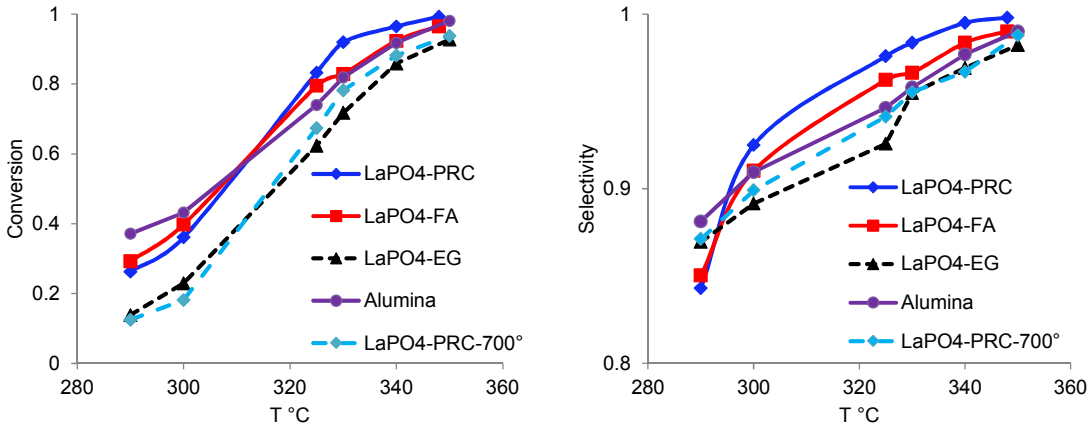

(a) (b)

Fig. 5. Ethanol dehydration conversion (a) and selectivity to ethylene (b) vs. temperature in the presence of $LaPO_4$ solids and alumina reference.

Comparison of the stability of the catalytic properties as a function of time on stream showed that intrinsic activity and ultra-selectivity of the rhabdophane sample were highly stable. The absence of strong acid sites, which are responsible for the formation of coke and the presence of water- accommodating "zeolitic" channels could explain their high selectivity and relative stability of hexagonal $LaPO_4$ polymorph. The deactivation of ethanol dehydration on $LaPO_4$-FA and $LaPO_4$-EG was greater than that on the open-framework $LaPO_4$-PRC (Fig. 6). Meanwhile, $LaPO_4$-FA, having the "aerogel" structure, performed significantly better than densely packed $LaPO_4$-EG. This confirms the influence of pore size on the catalyst's stability. Moreover, due to its open surface, the $LaPO_4$-PRC-700° monazite sample showed better stability than its microporous $LaPO_4$-EG counterpart (Fig. 6), despite greater specific surface area of the latter. Microporous $LaPO_4$-EG was the only sample that acquired a grayish color after catalytic test for 24h and contained 0.3% wt. of carbon according to HCNS elemental analysis.

In the previous paper [15] the catalytic properties, which are attributed to low or medium strength Brønsted acid sites, were found to be influenced by the bulk P/La ratio: high P/La ratio catalysts showed higher ethanol conversion and higher selectivity to ethylene. Here we see that at the strict La/P=1 ratio, a highly performing catalyst can be obtained. The crucial point seems to be phase purity and clean catalyst surface, devoid of extraneous species introduced by the preparation method.

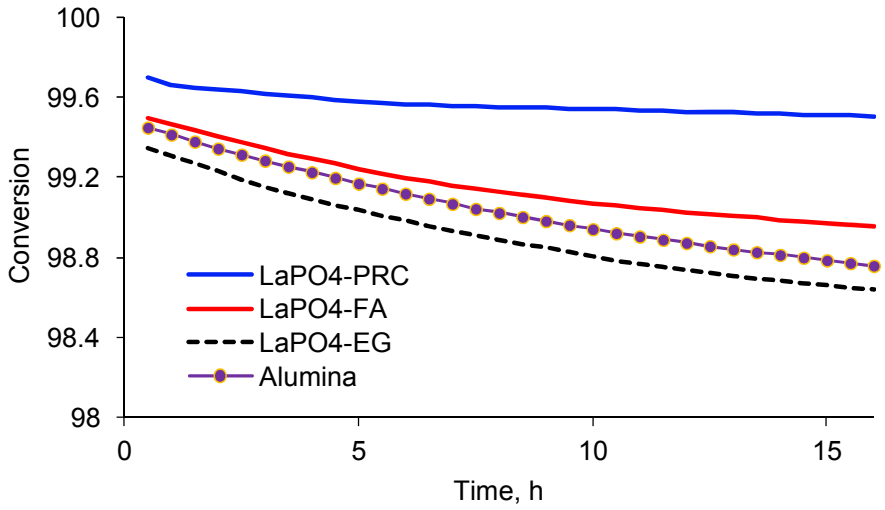

Fig. 6 Time evolution of ethanol conversion in the presence of $LaPO_4$ samples and reference alumina.

The distribution of Brønsted acid sites was investigated by TPD of NH_3. The NH_3–TPD profiles (Fig. 7) show strong desorption features peaking at 220-240 °C that reveal a rich amount of Brønsted acid sites on the surface of $LaPO_4$-based materials. Such sites are probably provided by the protons attached to surface phosphate groups. They have acidity depending on their coordination geometry, in turn related to the polymorph structure and to the indexes of the exposed facets, defined by particles shape. In lines with the previous paper [15] we attribute desorption ranges 100–250 °C, 250–400 °C and 400–600 °C to weak, medium and strong acid sites respectively ("very weak" sites from [15] are merged to "weak" ones as having no clear physical rationale). Three lanthanum phosphate catalysts contain mainly weak and medium sites. High temperature desorption tails might be attributed to some strong sites, more pronounced for monoclinic samples. $LaPO_4$-PRC has the weakest acid sites in the main TPD peak and the lowest amount of minority strong sites, whereas $LaPO_4$-EG has the strongest ones. Total amount of B sites and relative percentage of weak sites (% w.) is respectively 0.89 mmol/g (48% w.) in $LaPO_4$-PRC, 1.65 mmol/g (37% w.) for $LaPO_4$-FA and

1.24 mmol/g (34 %w.) for $LaPO_4$-EG. Moderate Lewis acidity has been also observed on the $LaPO_4$ phases in ref. [15], but no basic sites. The results of TPD of ammoniac clearly demonstrate that good catalytic performance and selectivity do not correlate to the strength of acidic sites, but require more specific properties, provided by rhabdophane but not by more acidic monazite. Overall activity is probably defined by balance of moderate acidic sites and sites geometry, yet unknown.

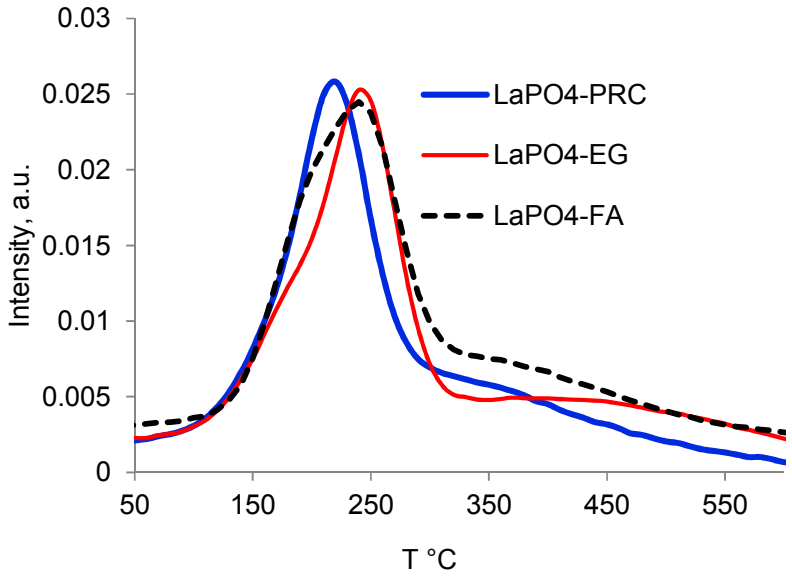

Fig. 7. NH_3 TPD patterns of the $LaPO_4$ catalysts.

4. Conclusions

Extremely simple room-temperature technique has been developed for the preparation of $LaPO_4$ that consists in several hours blending of ionic precursors in a polar solvent. Control of phase polymorph and morphology has been achieved by changing the nature of the non-aqueous solvent. The highest specific surface areas ever reported for the $LaPO_4$ solids have been obtained. Our catalytic tests demonstrated that the type of $LaPO_4$ polymorph plays a crucial role for high activity and ultra-selectivity in ethanol dehydration: hexagonal rhabdophane possesses advantageous properties whereas monoclinic monazite shows lower

performance. Beside the catalytic use, the preparation technique reported here provides a simple way to stable colloidal suspensions or monolith gels of $LaPO_4$. While monazite samples did not show high performance in the ethanol dehydration, due to exceptionally high surface area they might be interesting as catalysts or catalytic supports, e.g. for noble metals.[38]

Though optical materials are outside our scientific predilection, it seems quite probable that doped materials with advantageous properties will be easily prepared using this technique. Our preliminary results show that other phosphates can be prepared by non-aqueous metathesis technique, such as phosphates of Ca, Sr or Ba. Moreover, as our ongoing studies show, besides obtaining advantageous morphology, non-aqueous metathesis allows preparing wider scope of compounds, not available by straightforward aqueous precipitation, since in the aprotic and in many protic solvents hydrolysis (solvolysis) of metals ions does not proceed at all or is much less pronounced than in water.

Footnotes and references

[a] Institut de Recherches sur la Catalyse et l'Environnement de Lyon, IRCELYON, UMR 5256, CNRS – Université Lyon 1, 2, av. A. Einstein, 69626 Villeurbanne, France

pavel.afanasiev@ircelyon.univ-lyon1.fr

1 W. S. Song, K. H. Lee, Y. R. Do and H. Yang, *Adv. Funct. Mater.*, 2012, **22**, 1885.

2 J. A. Dorman, J. H. Choi, G. Kuzmanich and J.P. Chang, *J. Phys. Chem. C*, 2012, **116**, 12854.

3 U. Rambabu and S. Buddhudu, *Optic. Mater*. 2001, **17**, 401.

4 J. B. Davis, D. B. Marshall and P. E. D. Morgan, *J. Eur. Ceram. Soc*., 2000, **20**, 583.

5 P. E. D. Morgan and D. B. Marshall, *J. Amer. Ceram. Soc*., 1995, **78**, 1553.

6 S. S. Sujith, S. L. A. Kumar, R. V. Mangalaraja, A. P. Mohamed and S. Ananthakumar, *Ceram. Internat.,* 2014, **40**, 15121.

7 L. Malavasi, C. A. Fisher and M. S. Islam, *Chem. Soc. Rev.*, 2010, **39**, 4370.

8 T. Norby and N. Christiansen, *Solid State Ionics*, 1995, **77**, 240.

9 T. Anfimova, Q. F. Li, J.O. Jensen and N. Bjerrum, *Int. J. Electrochem. Sci*., 2014, **9**, 2285. 300.

10 A. Meldrum, L. A. Boatner and R. C. Ewing, *Phys. Rev. B*., 1997, **56**, 13805.

11 P. Afanasiev, M. Aouine, C. Deranlot, and T. Epicier, *Chem. Mater.*, 2010, **22**, 5411.

12 Y. Takita, K. Kurosaki, T. Ito, Y. Mizuhara and T. Ishihara, *Stud. Surf. Sci. Catal*., 1994, **90**, 441.

13 K. Rajesh, P. Shajesh, O. Seidel, P. Mukundan and K. G. K. Warrier, *Adv. Funct. Mater*., 2007, **17**, 1682.

14 B. Pan, S. Luo, W. Su and X. Wang, *Appl. Catal. B: Environmental* 2015, **168**, 458.

15 T. T. N. Nguyen, V. Ruaux, L. Massin, C. Lorentz, P. Afanasiev, F. Maugé, V. Bellière-Baca, P. Rey and J. M. M. Millet, *Appl. Catal. B: Environmental*, 2015, **166–167**, 432.

16 H. Meyssamy, K. Riwotzki, A. Kornowski, S. Naused and M. Haase, *Adv. Mater*.,1999, **11**, 840.

17 J. A. Diaz-Guillén, A. F. Fuente, S. Gallini and M. T. Colomer, J. Alloys Compds, 2007, **427**, 87.

18 M. G. Ma, F. Deng, K. Yao, *Mater. Lett*., 2014, **124**, 173.

19 C. Feldmann, *Adv. Func. Mater.*, 2003, **13**, 101.

20 M. Berbon, J. B. Davis, D. B. Marshall, R. M. Housley and P. E. D. Morgan, *Int. J. Mat. Res.*, 2007, **12**, 1244.

21 K. Riwotzki, H. Meyssamy, A. Kornowski, and M. Haase, J. Phys. Chem. B 2000, **104**, 2824.

22 M. T. Schatzmann, M. L. Mecartney and P. E. D. Morgan, *J. Mater. Chem*., 2009, **19**, 5720.

23 S. Bag, A. F. Gaudette, M. E. Bussell, M. G. Kanatzidis, Nature Chem., 2009, **1**, 217.

24 V. Sharma, F. Böhm, M. Seitz, G. Schwaab and M. Havenith, *Phys. Chem. Chem. Phys.* 2013, **15**, 8383.

25 A. Corma, S. Iborra and A. Velty, *Chem. Rev*., 2007, **107**, 2411.

26 C. B. Phillips and R. Datta, *Ind. Eng. Chem. Res*., 1997, **36**, 4466.

27 X. Zhang, R. Wang, X. Yang and F. Zhang, *Micropor. Mesopor. Mater*, 2008, **116**, 210.

28 K. Ramesh, L.M. Hui, Y.F. Han and A. Borgna, *Catal. Commun*., 2009, **10**, 567.

29 N. Zhan, Y. Hu, H. Li, D. Yu, Y. Han and H. Huang, *Catal. Commun*., 2010, **11**, 633–637.

30 J. H. Kwak, D. Mei, C. H. F. Peden, R. Rousseau and J. Szanyi, *Catal. Lett*., 2011, **141**, 649.

31 T. K. Phung, A. Lagazzo, M. A. Rivero Crespo, V. S. Escribano and G. Busca, *J. Catal.* 2014, **311**, 102.

32 V. T. Magalad, A. R. Supale, S. P. Maradur, G. S. Gokavi, T. M. Aminabhavi, *Chem. Eng. J.* 2010, **159**, 75.

33 D. P. Suhas, A. V. Raghu, H. M. Jeong and T. M. Aminabhavi, RSC Advances, 2013, 3, 17120.

34 H. Assaaoudi, A. Ennaciri, and A. Rulmont, *Vib. Spectrosc*. 2001, **25**, 81.

35 J. Ma and Q. Wu, *J. Appl. Cryst.,* 2010, **43**, 990.

36 P. Savchyn, I. Karbovnyk, V. Vistovskyy, A. Voloshinovskii, V. Pankratov, M. Cestelli Guidi, C. Mirri, O. Myahkota, A. Riabtseva, N. Mitina, A. Zaichenko and A. I. Popov, *J. Appl. Phys.*, 2012, **112**, 124309.

37 M. Salazar, D. A. Berry, T. H. Gardner, D. Shekhawat and D. Floyd, *Appl. Catalysis A: General*, 2006, **310**, 54.

38 W. F. Yan, S. Brown, Z. W. Pan, S. M. Mahurin, S. H. Overbury and S. Dai, *Angew. Chem. Int. Ed*. 2006, **45**, 3614.